Local structure analyses of $Ce_{0.5}Zr_{0.5}O_2$ mixed oxides by XAFS

Yasutaka Nagai,[a*] Takashi Yamamoto,[b] Tsunehiro Tanaka,[b] Satohiro Yoshida,[b] Takamasa Nonaka,[a] Tokuhiko Okamoto,[a] Akihiko Suda[a] and Masahiro Sugiura[a]

[a]Toyota Central R&D Labs., Inc., Nagakute, Aichi 480-1192, Japan, [b]Department of Molecular Engineering, Kyoto University, Kyoto 606-8501, Japan. Email:e1062@mosk.tytlabs.co.jp

Three types of CeO_2-ZrO_2 with the same composition (Ce/Zr = 1) were prepared by different methods, exhibited the different oxygen storage/release capacity (OSC). To investigate the relationship between the OSC and the local structure, the Ce and Zr K-edges XAFS spectra for these samples were measured. The features of Fourier transforms of these samples were different from each other. This suggested that the OSC was remarkably exerted by the local structure around Ce and Zr. The quantitative curve-fitting analysis of EXAFS was applied, and it was concluded that homogeneous $Ce_{0.5}Zr_{0.5}O_2$ solid solution at atomic level exhibited the highest OSC among these CeO_2-ZrO_2 with the same composition (Ce/Zr = 1).

Keywords: $Ce_{0.5}Zr_{0.5}O_2$, Oxygen Storage Capacity, Ce K-edge and Zr K-edge XAFS

1. Introduction

The oxygen storage/release capacity (OSC) is one of the important functions required for automobile three-way catalysts (TWCs) to remove harmful compounds such as hydrocarbons, CO and NOx in automotive exhaust gases (Matsumoto, 1994). In the TWCs, CeO_2 is widely used as a promoter due to its high OSC. Recently, it has been found in our laboratory that addition of ZrO_2 to CeO_2 could enhance the OSC of CeO_2 and thermal stability (Ozawa *et al.*, 1993). Therefore a considerable number of studies have been made on the structure of CeO_2-ZrO_2 (e.g., Omata *et al.*, 1999), but detailed information remains unclear. Also XAFS studies have been made for the purpose of the investigation on the local structure around Ce and Zr. All of these XAFS studies utilize Ce L_{III}-edge (e.g., Vlaic *et al.*, 1997), and no studies employing Ce K-edge XAFS have been reported. The *k*-range of Ce L_{III}-edge EXAFS is limited to ca. 3 - 9 $Å^{-1}$, because of the presence of Ce L_{II}-edge in high-energy region. Since Ce and Zr contributions to EXAFS signals are remarkable in high-*k* part (Teo, 1986), a wide *k*-range is necessary to obtain the precise information on Ce-Ce and Ce-Zr bonding. In the present work, we measured Ce K-edge and Zr K-edge XAFS spectra of three types of CeO_2-ZrO_2 with the same composition (Ce/Zr = 1), which exhibited the different OSC efficiency. The purpose is to clarify the relationship between the OSC and the local structures around Ce and Zr, mainly cation-cation (cation = Ce, Zr) network, of these samples.

2. Experimental

Three types of CeO_2-ZrO_2 with the same composition (Ce/Zr = 1; CZ55-1, CZ55-2 and CZ55-3) were prepared by the following methods. CZ55-1 was prepared by the precipitation process using CeO_2 powder (Anan Kasei Co. Ltd.) and $ZrO(NO_3)_2$ aqueous solution as starting materials. CZ55-2 was prepared by the coprecipitation process using $Ce(NO_3)_3$ and $ZrO(NO_3)_2$ aqueous solutions as starting materials. CZ55-1 and CZ55-2 were calcined at 773 K. CZ55-3 was synthesized by the same coprecipitation process as CZ55-2, followed by heating at 1473 K under reductive condition. All the samples were calcined at 773 K for 3 h before XAFS and X-ray diffraction measurements. Oxygen was fully stored into Ce compounds with this treatment.

The OSC of 1 wt% platinum loaded CeO_2-ZrO_2 samples were estimated by the measurements of the weight change with the oxygen storage/release under oxidative/reductive conditions using a thermogravimetry apparatus.

Powder XRD measurement was carried out on RINT2000 (Rigaku Co. Ltd.) diffractometer using Cu-Kα radiation to characterize the solid phase of CeO_2-ZrO_2 samples.

Ce K-edge (40.45 keV) and Zr K-edge (18.00 keV) XAFS spectra of these samples were measured at BL01B1 and BL16B2 of SPring-8. The storage ring energy was operated at 8 GeV with a typical current of 100 mA. Measurements were carried out in a transmission mode at room temperature with a Si(311) double crystal monochromator. Normalization of XANES and data reduction on EXAFS were carried out as described elsewhere (Tanaka *et al.*, 1988). The quantitative curve-fitting analysis of the EXAFS spectra was performed for the inverse Fourier transforms on cation-cation (cation = Ce, Zr) shells. Empirical parameters in the analysis were obtained from standard compounds, e.g. CeO_2 for Ce-Ce bonding, 8 mol% Y-doped cubic ZrO_2 for Zr-Zr bonding, and cubic $Ce_{0.9}Zr_{0.1}O_2$ for Zr-Ce bonding. A parameter for Ce-Zr bonding was calculated from the extracted Ce-Ce, Zr-Zr and Zr-Ce parameters.

3. Results and discussion

The OSC of the samples at 773 K was in the order of CeO_2 (0.05 mmol-O_2/g) ≈ CZ55-1 (0.08 mmol-O_2/g) < CZ55-2 (0.44 mmol-O_2/g) < CZ55-3 (0.75 mmol-O_2/g). Thus CZ55-3 exhibited the highest OSC.

From the XRD pattern (data not shown), CZ55-1 was found as the mixture of cubic CeO_2 and tetragonal ZrO_2, although CZ55-2 and CZ55-3 could be found as the cubic phase of $Ce_{0.5}Zr_{0.5}O_2$ (Omata *et al.*, 1999).

Figs. 1 and 2 show Ce and Zr K-edges EXAFS spectra of the samples, respectively. The spectra with a good signal-to-noise ratio at both of Ce and Zr K-edges were obtained in the wide region of 3.0 - 17.0 $Å^{-1}$. At the high-*k* part 9.0 - 17.0 $Å^{-1}$ of Ce K-edge, we could observe the apparent EXAFS signals caused mainly by Ce and/or Zr. Ce K-edge EXAFS signals of CZ55-1, CZ55-2 and CZ55-3 are obviously different from each other. On the other hand, the spectrum of CZ55-1 is very similar to that of CeO_2 in points of frequencies and amplitudes. Also the Zr K-edge EXAFS spectra of the CeO_2-ZrO_2 samples have different features respectively.

Fourier transformations (FTs) were performed on Ce and Zr K-edges EXAFS spectrum in about 3.0 - 17 $Å^{-1}$ region. The FTs of the Ce K-edge EXAFS spectra are presented in Fig. 3. The first peak at 1.8 Å corresponds to Ce-O bonds and the second peak at 3.5 Å to Ce-cation (cation = Ce, Zr) bonds. The Ce-O and Ce-cation peaks of CZ55-1 are located almost at the same positions as those of CeO_2, and have the same amplitudes. While the position and amplitude of the Ce-O peaks for CZ55-1, CZ55-2 and CZ55-3 are slightly different from each other. The Ce-cation peaks of CZ55-2 and CZ55-3 have lower amplitudes than that of CZ55-1. It should be noted that the Ce-cation peak of CZ55-3 seems to split into two peaks. These clear differences for the Ce-cation peaks could not be observed in Ce L_{III}-edge

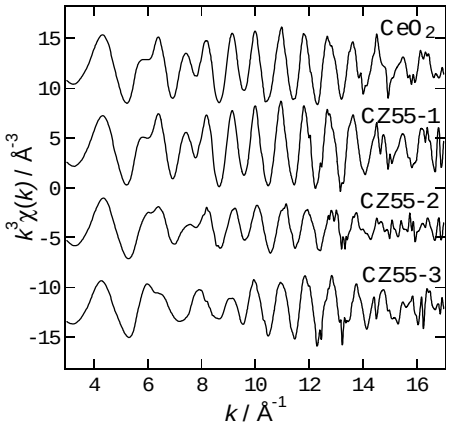

Figure 1
The k^3-weighted Ce K-edge EXAFS spectra. For sample denotation, see Experimental.

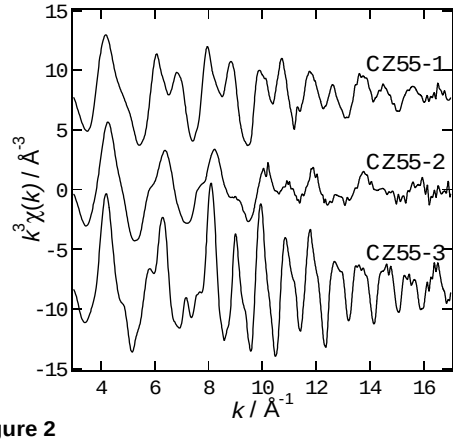

Figure 2
The k^3-weighted Zr K-edge EXAFS spectra.

(data not shown). Therefore the measurements of Ce K-edge XAFS spectrum are necessary to obtain the precise information on Ce-cation bonding. Fig. 4 shows the FTs of the Zr K-edge EXAFS spectra. The first peak at 1.7 Å was assigned to Zr-O bonds and the second peak at 3.5 Å to Zr-cation bonds. The FTs of CZ55-1, CZ55-2 and CZ55-3 are obviously different in their shape. According to the results mentioned above, it is suggested that the OSC have a significant correlation with the local structure around Ce and Zr.

The XANES spectra at Zr K-edge are shown in Fig. 5. Comparison of the spectra indicated by the *A* or *B* was made carefully. To begin with, peak *A*, a weak shoulder on the steeply rising absorption edge, is more apparent in CZ55-1 and CZ55-2 than in CZ55-3. This pre-edge absorption can be assigned to $1s \rightarrow 4d$ transition which is stronger for the lower symmetry of Zr-O coordination, and appears pronouncedly for pure tetragonal ZrO_2 (Li *et al.*, 1993a). In fact, the feature of the XANES spectrum of CZ55-1 is very similar to that of pure tetragonal ZrO_2 (Li *et al.*, 1993a). Next, the peak *B* in CZ55-1 shows a single broad peak, whereas that in CZ55-2 shows a slight splitting into two peaks, and in CZ55-3 a clear splitting. A similar splitting has been reported for Y_2O_3-ZrO_2 solid solution (Li *et al.*, 1993b). Li *et al.* have reported that the splitting becomes progressively more pronounced as the Y_2O_3 concentration in Y_2O_3-ZrO_2 solid solution increases from 3 mol% to 20 mol%, additionally, and that peak *A* decreases with

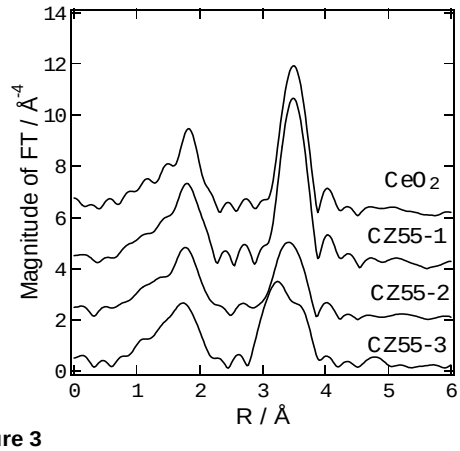

Figure 3
Fourier-transformed $k^3\chi$ data at Ce K-edge.

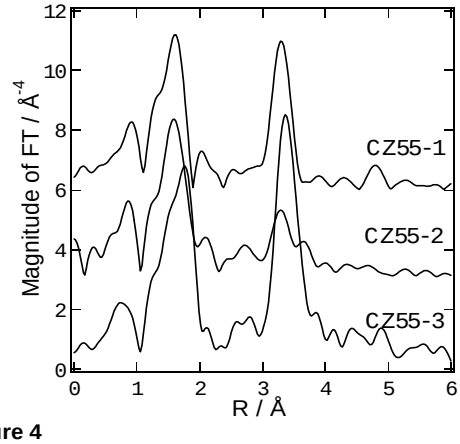

Figure 4
Fourier-transformed $k^3\chi$ data at Zr K-edge.

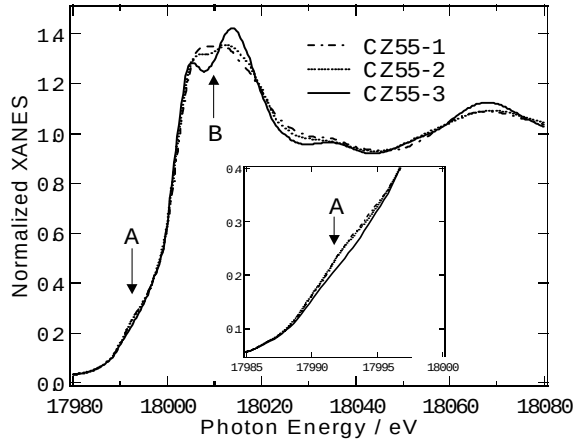

Figure 5
Zr K-edge normalized XANES spectra.

increasing the Y_2O_3 concentration. Therefore the results of these XANES spectra in this system indicate that the concentration of Ce insertion into ZrO_2 increases along the series: CZ55-1, CZ55-2 and CZ55-3.

Table 1
Results of curve-fitting analysis of Ce K-edge EXAFS.

	Shell	CN [a]	R [a] / Å	$\Delta\sigma^{2}$ [a, b] / Å^2
cubic CeO_2 [c]	Ce-Ce	12	3.826	
CZ55-1	Ce-Ce	11.9(2)	3.82(0)	0.0026(1)
CZ55-2	Ce-Ce	8.0(4)	3.78(0)	0.0034(2)
	Ce-Zr	3.6(5)	3.71(0)	0.0063(13)
CZ55-3	Ce-Ce	6.0(3)	3.78(0)	0.0016(2)
	Ce-Zr	6.0(3)	3.72(0)	0.0022(3)

[a] The standard deviation is given in parentheses.
[b] Relative Debye-Waller factor
[c] Standard compound

Table 2
Results of curve-fitting analysis of Zr K-edge EXAFS.

	Shell	CN [a]	R [a] / Å	$\Delta\sigma^{2}$ [a, b] / Å^2
cubic ZrO_2 [c]	Zr-Zr	12	3.599	
CZ55-1	Zr-Zr	6.6(2)	3.66(0)	0.0061(2)
CZ55-2	Zr-Zr	3.0(6)	3.69(0)	0.0124(19)
	Zr-Ce	4.0(3)	3.76(0)	0.0030(3)
CZ55-3	Zr-Zr	6.0(4)	3.62(0)	0.0086(6)
	Zr-Ce	6.0(3)	3.75(0)	-0.0010(1)

[a] The standard deviation is given in parentheses.
[b] Relative Debye-Waller factor
[c] 8 mol% Y-doped cubic ZrO_2 as standard compound

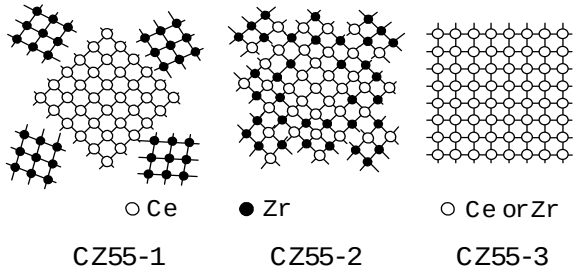

Figure 6
Model illustration of cation-cation network for the CeO_2-ZrO_2 samples with the same composition (Ce/Zr = 1). CZ55-1 consists of of pure CeO_2 and ZrO_2. Ce rich domain and Zr rich one in CZ55-2 still remain. $Ce_{0.5}Zr_{0.5}O_2$ solid solution in CZ55-3 forms homogeneously at atomic level.

The quantitative curve-fitting results of Ce and Zr K-edges EXAFS are summarized in Tables 1 and 2, respectively. Only results for cation-cation bonding around 3.0 - 4.0 Å in the FTs are presented here to focus on cation-cation network in CeO_2-ZrO_2. Our data-fitting procedure began with the reference to coordination numbers and distances of cation-cation bonding for cubic CeO_2 and ZrO_2 polymorphs (cubic, tetragonal and so on), which were determined by XRD (Li *et al.*, 1993a). First, the Ce-cation shell for CZ55-1 was fitted with a single Ce-Ce shell, and the Zr-cation shell also was fitted with a single Zr-Zr shell. The distance (R = 3.82 Å) and coordinaion number (CN = 11.9) of the Ce-Ce shell is consistent with the values for CeO_2. Thus CZ55-1 consists of pure CeO_2 and ZrO_2, and CeO_2-ZrO_2 solid solution hardly forms. The CN = 6.6 of the Zr-Zr shell for CZ55-1 is lower than 12. It could be considered that the size of formed ZrO_2 crystallite was small. Secondly, in the case of CZ55-2, not only Ce-Ce and Zr-Zr shells but also Ce-Zr and Zr-Ce shells were necessary to obtain the appropriate fit for the cation-cation shell (at Ce and Zr K-edges, respectively). The Ce-cation shell was fitted with Ce-Ce (CN = 8.0) and Ce-Zr (CN = 3.6) shells. The CN of the Ce-Ce shell is larger than that of the Ce-Zr shell. The CN = 3.6 of the Ce-Zr shell is close to the CN = 4.0 of Zr-Ce shell. This indicates that CeO_2-ZrO_2 solid solution in CZ55-2 forms partially, but Ce rich domain and Zr rich one still remain. As to single Zr-Zr shell of CZ55-2, we could not obtain the appropriate fit. The relative Debye-Waller factor ($\Delta\sigma^2$) is so large. This may mean that the distribution of Zr-Zr bond distances is broad because of the presence of a structural disorder. Finally, the Ce-cation shell for CZ55-3 was fitted with Ce-Ce (CN = 6.0) and Ce-Zr (CN = 6.0) shells. The Zr-cation shell also was fitted with Zr-Zr (CN = 6.0) and Zr-Ce (CN = 6.0) shells. The evaluated values correspond with the Ce/Zr composition ratio = 1 of the sample. It is clear that $Ce_{0.5}Zr_{0.5}O_2$ solid solution in CZ55-3 forms homogeneously at atomic level. The homogeneity of CeO_2-ZrO_2 solid solution increases in the order of CZ55-1, CZ55-2 and CZ55-3. This is agreement with the suggestion derived from the result of the Zr K-edge XANES. On the grounds of above results, the model illustration of cation-cation network for the CeO_2-ZrO_2 samples is shown in Fig. 6.

It is concluded from the present study that the OSC is remarkably exerted by the local structure around Ce and Zr, and that homogeneous $Ce_{0.5}Zr_{0.5}O_2$ solid solution at atomic level exhibited the highest OSC. Additionally, Ce K-edge XAFS provides the precise information on Ce-cation bonding.

The reason why the OSC increases with increasing the homogeneity of CeO_2-ZrO_2 solid solution has not been clarified. To make this point clear, further we need to investigate the oxygen storage/release behavior on homogeneous CeO_2-ZrO_2 solid solution by XAFS.

The X-ray absorption experiments were performed at the SPring-8 with the approval of the Japan Synchrotron Radiation Research Institute (JASRI) (Proposal No. 2000A0143-NX-np & C99B16B2-417N).

References

Matsumoto, S. (1994). *Toyota Tec. Rev.* **44**, 10-15.
Ozawa, M., Kimura, M. & Isogai, A. (1993). *J. Alloys Comp.* **193**, 73-75.
Omata, T., Kishimoto, H., Otsuka-Yao-Matsuo, S., Ohtori, N. & Umesaki, N. (1999). *J. Solid. State Chem.* **147**, 573-583.
Vlaic, G., Fornasiero, P., Geremia, S., Kašpar, J. & Granziani M. (1997). *J. Catal.* **168**, 386-392.
Teo, B. K. (1986). *EXAFS: Basic Principles and Data Analysis*, Springer-Verlag, Berlin.
Tanaka, T., Yamashita, H., Tsuchitani, R., Funabiki, T. & Yoshida, S. (1988). *J. Chem. Soc., Faraday Trans. I* **84** 2987-2999.
Li, P., Chen, I-W., Penner-Hahn, J. E. (1993a). *Phys. Rev. B* **48**, 10063-10073.
Li, P., Chen, I-W., Penner-Hahn, J. E. (1993b). *Phys. Rev. B* **48**, 10074-10081.